Coordination-resolved local bond relaxation, electron binding-energy shift, and Debye temperature of Ir solid skins

Maolin Bo,[a] Yan Wang,[a,b] Yongli Huang,[a*] Xuexian Yang,[c] Yezi Yang,[a] Can Li,[d] Chang Q Sun[a,e*]

[a]*Key Laboratory of Low-Dimensional Materials and Application Technologies, Ministry of Education, Xiangtan University, Hunan 411105, China*

[b]*School of Information and Electronic Engineering, Hunan University of Science and Technology, Hunan 411201, China*

[c]*Department of Physics, Jishou University, Jishou, Hunan 416000, China*

[d]*Center for Coordination Bond Engineering, School of Materials Science and Engineering, China Jiliang University, Hangzhou 330018, China*

[e]*NOVITAS,School of Electrical and Electronic Engineering, Nanyang Technological University, Singapore 639798, Singapore*

*E-mail:huangyongli@xtu.edu.cn; ecqsun@ntu.edu.sg

Abstract

Numerical reproduction of the measured $4f_{7/2}$ energy shift of Ir(100), (111), and (210) solid skins turns out the following: (i) the $4f_{7/2}$ level of an isolated Ir atom shifts from 56.367eV to 60.332 eV by 3.965 eV upon bulk formation; (ii) the local energy density increases by up to 130% and the atomic cohesive energy decreases by 70% in the skin region compared with the bulk values. Numerical match to observation of the temperature dependent energy shift derives the Debye temperature that varies from 285.2 K (Surface) to 315.2 K (Bulk). We clarified that the shorter and stronger bonds between under-coordinated atoms cause local densification and quantum entrapment of electron binding energy, which perturbs the Hamiltonian and the core shifts in the skin region.

Keywords: XPS, Ir surface, BOLS, tight binding

1 Introduction

Low-dimensional systems such as adatoms, nanowires, nanotubes, nanograins, stepped surfaces and the skin of a flat surface have inspired increasing interests because of their novel chemical and physical properties [1-6]. These low-dimensional systems are characterized by high fractions of under-coordinated atoms [7, 8]. The noble metal Ir [9] and its binary alloy [10] are good catalysts. However, detailed knowledge of the local bond attribute, atomic cohesive energy, binding energy density in the skin are of great importance but poorly known. Furthermore, the underlying mechanism for the unusual behavior of Ir skins remains unclear though it is often referred to the variation of surface-to-volume ratio [11] and the energy shift to the "initial-final states" relaxation in the process of ionization and excitation [12]. Therefore, an atomistic understanding of the bond nature and thermal effect on the binding energy shift in the skin, and a method purifying the spectral information confined within the outermost one or two atomic layers is highly desired [13-18].

In this work, we report our findings in analyzing the X-ray photoelectron spectroscopy (XPS) profiles of Ir $4f_{7/2}$ surfaces based on the framework of BOLS (bond order-length-strength) correlation notation and tight-binding (TB) theory [19]. We considered the effects of temperature, crystal orientation, and layer order on the energy shifts in the skin region from the perspective of Hamiltonian perturbation by the local bond relaxation and the associated quantum entrapment.

2 Principles

2.1 Tight binding approximation

According to the band theory [1], the integral of the intra-atomic potential, $V_{\text{atom}}(\text{r})$, and the respective eigenwave function of an atom at the specific ith atomic site, $|v,i\rangle$, determines the vth energy level of an isolated atom, $E_v(0)$. The involvement of the interatomic potential $V_{\text{cry}}(\text{r})$ shifts the $E_v(\text{z} = 0)$ deeper by an amount that is proportional to the cohesive energy per bond at equilibrium following the expression [20] with z being the effectively atomic coordination numbers (CNs),

$$E_v(0) = \langle v,i|V_{atom}(r)|v,i\rangle$$

$$\Delta E_v(12) = E_v(12) - E_v(0) = \langle v,i|V_{cry}(r)|v,i\rangle + \sum_{j=1}^{j=z}\langle v,i|V_{cry}(r)|v,j\rangle$$
$$= \alpha(1+\frac{z\beta}{\alpha}) \cong \alpha \propto E_b \quad (1)$$

The coordination number z = 0 and 12 represents an isolated atom and an atom in the bulk, respectively. The sum is over all z neighbors of the specific ith atom. The α is the exchange integral and β the overlap integral. Because $\langle v,i|v,j\rangle = \delta_{ij}$ with δ_{ij} being the Kronig function (if i = j,δ_{ij} = 1, otherwise, δ_{ij} = 0),the $z\beta/\alpha$ << 1. Any perturbation to the bond energy E_b will shift the core level accordingly.

2.2 BOLS correlation

According to the BOLS correlation [1], atomic undercoordination shortens and strengthens the remaining bonds between undercoordinated atoms, which follow the expressions: $d_i = C_z d_b = 2d_b / \{1+\exp[(12-z_i)/8z_i]\}$ and $E_i = C_z^{-m} E_b$,where C_z is the coefficient of bond contraction with z_i being the effective coordination of an atom in the ith atomic layer. The i counts from the outermost layer inward up to three. The bond nature indicator m correlates the bond energy to the bond length. For most metals, m=1[1]. Any factor that affects the bond length and energy shifts potential well and the core level accordingly. Incorporating the BOLS into the TB approximation yields,

$$V_{cry}(\Delta_H) = V_{cry}(r)[1+\Delta_H]$$

Where

$$\Delta_H = \begin{cases} C_z^{-m} - 1 & \text{(Surface effect)} \\ \dfrac{\int_0^T \eta(T)dt}{E_z} & \text{(thermal effect)} \end{cases} \quad (2)$$

2.2.1 Surface effect

With respect to the bulk shift $\Delta E_v(12)$, the under-coordination induced core level shifts (CLSs), $\Delta E_v(z)$, follows:

$$\frac{\Delta E_v(z)}{\Delta E_v(12)}=\frac{E_v(z)-E_v(0)}{E_v(12)-E_v(0)}=\frac{E_z}{E_b}=C_z^{-1}$$

(3)

With the given XPS spectral components related to z and z′, one can determine the referential $E_v(0)$, the bulk shift, $\Delta E_v(12)$, and the z dependent shift using **eq(3)**:

$$\frac{E_v(z)-E_v(0)}{E_v(z')-E_v(0)}=\frac{C_z^{-1}}{C_{z'}^{-1}}\ (z'\neq z)\ \ or\ \ E_v(0)=\frac{C_{z'}E_v(z')-C_zE_v(z)}{C_{z'}-C_z}\quad (z'\neq z)$$

$$E_v(z)=E_v(0)+\left[E_v(12)-E_v(0)\right]C_z^{-1}$$

(4)

2.2.2 Thermal effect

When the testing temperature is raised, the length and the strength of the representative bond will change. If the effects of atomic CN and temperature come into play simultaneously, the length, $d(z,T)$, and the bond energy, $E(z,T)$, of the representative bond will change accordingly. Therefore, based on the local bond average approach, the BOLS evolves into,

$$\begin{cases} d(z,T)=d_b\left[\left(1+\left(C_z-1\right)\right)\left(1+\int_{T_0}^{T}\alpha(t)\,dt\right)\right] \\ E(z,T)=E_b\left[1+\dfrac{\left(C_z^{-m}-1\right)-\int_{T_0}^{T}\eta(t)\,dt}{E_b}\right] \end{cases}$$

(5)

T_0 is the reference at the ambient conditions. The $\alpha(t)$ is the temperature dependent thermal expansion coefficient. $\eta(t)$ is the T-dependent specific heat of the representative bond, which follows Debye approximation, $C_v(T/\theta_D)$, for a z-coordinated atom. Generally, the thermal measurement is conducted under constant pressure and the η(t) should be related to the C_p. However, there is only a few percent difference between the C_p and C_v [19].

The bond energy approximates linearly at $T > \theta_D$, $E_b = \eta_1 T_m + \eta_2$ with η_1 being the constant specific heat per bond and η_2 the $1/z_b$ fold of latent heat for atomization of an atom

in molten state. Considering the fact that the melting point at the *i*th atomic site, T_{mi} is proportional to atomic cohesive energy, $T_{mi} \propto z_i E_i$, we have the relation $T_{mi} / T_m = z_i E_i / z_b E_b = z_{ib} C_i^{-m} = 1 + \Delta_T$ with Δ_T being the perturbation to the atomic coherency. The $z_{ib} = z_i / z_b$ is the normalized atomic coordination with $z_b = 12$ being the standard value in fully coordinated system. Then, we have the relation $T_{mi} = z_{ib} C_i^{-m} T_m = T_m (1 + \Delta_T)$ and $E_i = \eta_{1i} T_{mi} + \eta_{2i} = C_i^{-m} E_b = C_i^{-m} (\eta_1 T_m + \eta_2)$ [21].

According to Debye approximation, the thermal perturbation to the cohesive energy follows the relationship,

$$\Delta_T = \frac{\int_0^T \eta(T) dt}{E_z} = \int_0^T \frac{C_V(T/\theta_D)}{z E_z} dt = \frac{\tau^2 R}{E_{coh}} \left(\frac{T}{\theta_D} \right)^{\tau} \int_0^T \int_0^{\theta_D / T} \frac{x^{\tau+1} e^x}{(e^x - 1)^2} dx dt \qquad (\tau = 1, 2, 3) \tag{6}$$

Where $E_{coh} = zE_z$ is the atom cohesive energy to be determined in the fitting. τ is the shape factor (τ = 1, 2, and 3 corresponds to a thin plate, a cylindrical rod, and a sphere dot, respectively). The specific heat $\eta(T)$ per bond approximates the Debye scheme and closes to a constant value of τR (R is the ideal gas constant) at high temperatures. θ_D and C_v are the Debye temperature and the specific heat, respectively.

3 Results and Discussion

3.1 Skin-resolved quantum entrapment

According to the BOLS-TB notation on the energy separation between each component, **eq(4)**, each XPS spectrum is decomposed into the bulk (B) and surface (S_i) components from higher (smaller value) to lower BE upon background correction. The decomposition was conducted by referring the z values of fcc(100) and the fcc(111) surfaces as the standard [22]. The z values for the fcc(210) for the rest components were optimized together with the fine tuning of the peaks of all components. The number of components is taken with respect to the originally reported count but the peak energies are subject to adjustment to fit the overall

peak intensity. The optimal component energies, the intensities, and the corresponding z_i values of the XPS $4f_{7/2}$ data for Ir surfaces can be obtained in the fitting of the spectra after the Shirley background correction, as summarized in Table 1.

The $4f_{7/2}$ spectra collected from Ir(100)[23], (111)[16], and (210)[24] clean surfaces, as shown in Fig.1. The spectra were decomposed into the B, the first and the second surfaces (S_1, S_2) and the kink edge (S_E) for (210) surface. Including the common B component (z = 12), there are a total of 8 components for the Ir surfaces at quest. There will be a combination of $N=28=C_l^2=l!/[(l-2)!2!]$ values of $E_v(0)$. Using the least-root-mean-square approach, we can find the average of $\langle E_v(0)\rangle=\sum_N\langle E_{vi}(0)\rangle/N$ and the standard deviation. A fine-tuning of the CN values will minimize the σ and hence improve the accuracy of the effective CNs, the local bond strain, the BE density, and the cohesive energy per discrete atom in differently oriented surface layers, as shown in Table 1. Fig.2 show the CN-resolved bond strain, bond energy, energy density and atomic cohesive energy of Ir skins, which are critical to the performance of Ir. For instance, bond energy gain deepens the core level and hence enlarges the electroaffinity and chemical reactivity; energy density gain raises the local elasticity; cohesive energy loss lowers the thermal stability, accordingly.

The z-resolved $4f_{7/2}$ shift follows the relationship with $E_v(0)$ and $E_v(12)$ being intrinsic constants, regardless of crystal orientations or chemical environment:

$$E_{4f_{7/2}}(z)=\left\langle E_{4f_{7/2}}(0)\right\rangle\pm\sigma+\Delta E_{4f_{7/2}}(12)C_z^{-m}=56.367\pm0.006+3.965/C_z$$

This information is of great importance in understanding the surface behavior of these under-coordinated atoms.

3.2 Thermal effect

Using XPS data and the predicted trend of BE Shift [16] in eq(6) we can resolve the Debye temperatures. In the numerical calculations, we took the known CNs of Ir (111) surface and Debye temperature (θ_D) at 0 K and under the atmospheric pressure from the literature as input [25-27]. Only one fitting parameter of the E_z is used. Otherwise, the θ_D is a fitting parameter of interest. Fig.3 shows the theoretical reproduction of the measured

temperature-dependent CLSs of Ir with different E_z. The calculation was conducted with **eq (6)**, when the measuring temperature $T < \theta_D/3$, the small change arises from the small $\int \eta(t)dt$ values as the specific heat $\eta(t)$ is proportional to T^3. When the measuring temperature $T \geq \theta_D/3$, the specific heat C_v approaches a constant value of 3R (R is the idea gas constant) according to Debye approximation, the changes of BE always turn from nonlinear to linear when the temperature is increased.

The results imply that the θ_D determines the width of the shoulder and the inverse of the atomic cohesive energy $[zE_z(i)]^{-1}$ determines the slope of the BE curve at high temperatures. The BE shifts due to the temperature-dependence of bond relaxation. The similarity of the predict trend to those of the temperature-dependent Raman shift and Young's modulus of other materials [21] evidence the generality of the current approaches to the thermally induced property change of solid materials.

4 Conclusion

We have analyzed the Ir $4f_{7/2}$ energy shift of the (001), (111) and (210) surfaces from the perspective of bond–potential–band correlation and elucidated information regarding: (i) the $4f_{7/2}$ core level energy of an isolated Ir atom and its bulk shift, (ii) the effective atomic CNs and the corresponding local strains, (iii) prediction of the trends of coordination resolved binding energy density and cohesive energy per discrete atom in the skin, and, (iv) the temperature effect on energy shifts as arising from perturbation by the response of the length and energy of the representative bond. The concepts of local strain, quantum entrapment may be essential for understanding the bonding and electronic behavior in the surface and atomic defect sites.

Acknowledgment

Financial support from NSF(Nos. 11242005 and 11172254) and Scientific Research Fund of Hunan Provincial Education Department (Grant No.12C0132)

Tables and Figure captions

Table 1 The effective CN(z), lattice strain (ε_z = C_z-1 (%)), relative BE shift ($\delta E_z = \Delta E(z)/\Delta E(12) - 1 = \left(C_z^{-1} - 1\right)(\%)$), relative atomic cohesive energy (E_C = $E_C(z)/E_C(12)$-1= $\left(z_{ib} C_z^{-1} - 1\right)(\%)$), and the relative BE density (E_D = $E_D(z)/E_D(12)$= $\left(C_z^{-4} - 1\right)(\%)$)in various registries of Ir skins.

	i	$E_{4f7/2}$	z	-ε_z(%)	δE_z	-δE_C	δE_D
Bulk	B	60.332	12.00	0	0	0	0
Ir(100)	S_2	60.624	5.73	6.83	7.33	48.75	32.70
	S_1	60.898	4.00	12.44	14.20	61.93	70.09
Ir(111)	S_2	60.571	6.31	5.63	5.97	44.28	26.08
	S_1	60.840	4.26	11.31	12.75	59.97	61.60
Ir(210)	S_2	60.613	5.83	6.60	7.07	47.98	31.43
	S_1	60.861	4.16	11.72	13.28	60.73	64.68
	S_E	61.251	2.97	18.78	23.12	69.53	129.77

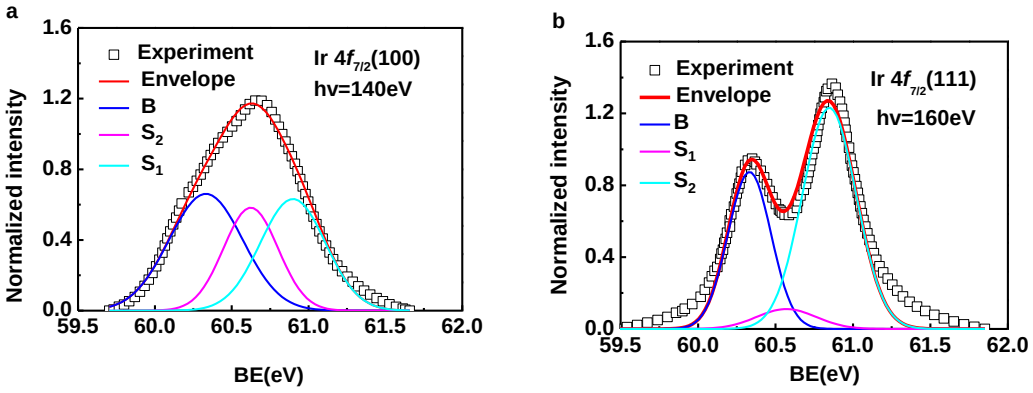

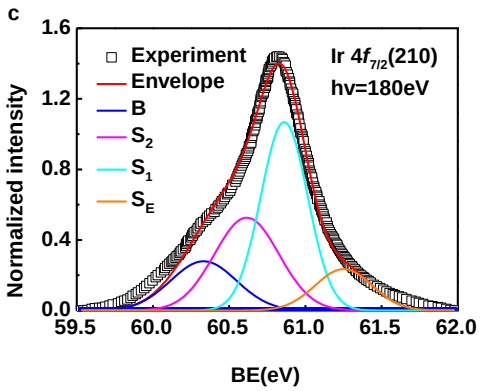

Fig.1 Decomposed XPS spectra for (a) the Ir(100)[23], (b) (111)[16], and (c)(210)[24] surfaces with derived information as summarized in Table 1. The $4f_{7/2}$ core level of 60.332±0.006eV and the B component at 60.332 should be identical for all the surfaces of the same material.

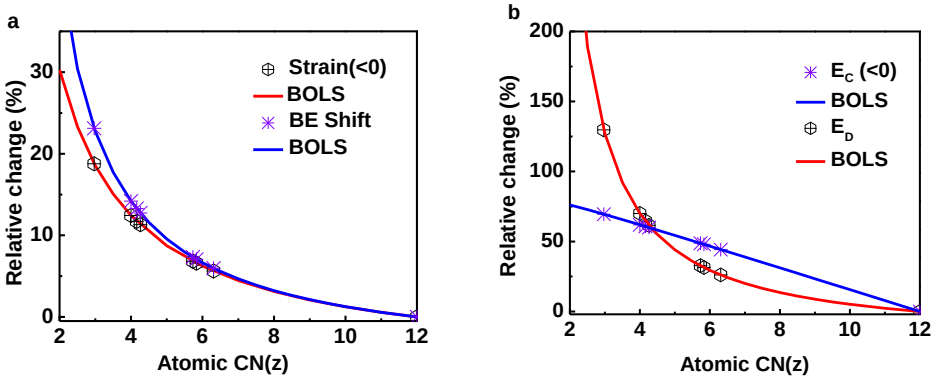

Fig.2 Coordination number (z) resolved (a) local bond strain and BE shift (entrapment) (b) atomic cohesive energy E_C and binding energy density E_D.

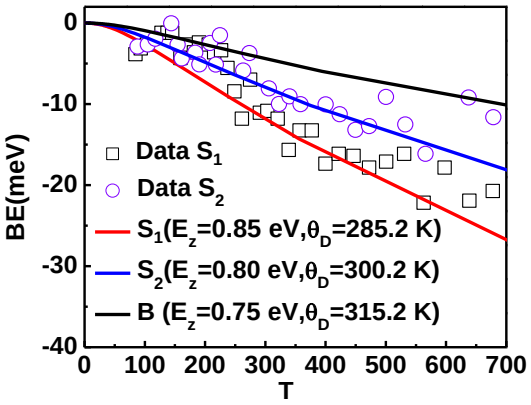

Fig.3 Coordination-resolved bond energy and Debye temperature for the surface sublayers derived from fitting to the measurements with the known θ_D=315.2K [25-27] as input parameters for Ir(111) surface. The accuracy can be improved with provision of the layer resolved spectral data.

References

[1] C.Q. Sun, Relaxation of the Chemical Bond, Heidelberg New York Dordrecht London Singapore 2014
[2] Ç.Ö. Girit, J.C. Meyer, R. Erni, M.D. Rossell, C. Kisielowski, L. Yang, C.-H. Park, M.F. Crommie, M.L. Cohen, S.G. Louie, A. Zettl, Graphene at the Edge: Stability and Dynamics, Science, 323 (2009) 1705-1708.
[3] W.J. Huang, R. Sun, J. Tao, L.D. Menard, R.G. Nuzzo, J.M. Zuo, Coordination-dependent surface atomic contraction in nanocrystals revealed by coherent diffraction, Nat Mater, 7 (2008) 308-313.
[4] J.G. Chen, C.A. Menning, M.B. Zellner, Monolayer bimetallic surfaces: Experimental and theoretical studies of trends in electronic and chemical properties, Surface Science Reports, 63 (2008) 201-254.
[5] Q. Jiang, L.H. Liang, D.S. Zhao, Lattice Contraction and Surface Stress of fcc Nanocrystals, The Journal of Physical Chemistry B, 105 (2001) 6275-6277.
[6] S. Xiong, W. Qi, B. Huang, M. Wang, Z. Li, S. Liang, Size–Temperature Phase Diagram of Titanium Nanosolids, The Journal of Physical Chemistry C, 116 (2011) 237-241.
[7] J. Pan, G. Liu, G.Q. Lu, H.-M. Cheng, On the True Photoreactivity Order of {001}, {010}, and {101} Facets of Anatase TiO2 Crystals, Angewandte Chemie International Edition, 50 (2011) 2133-2137.
[8] X.-Q. Gong, A. Selloni, M. Batzill, U. Diebold, Steps on anatase TiO2(101), Nat Mater, 5 (2006) 665-670.
[9] J. Li, G. Wu, N. Guan, L. Li, NO selective reduction by hydrogen over bimetallic Pd–Ir/TiO2 catalyst, Catalysis Communications, 24 (2012) 38-43.
[10] H. Zhang, Y. Liu, M. Zhang, Y. Li, Emission and surface characteristic of ternary alloy Ir/Re/W-coated impregnated tungsten cathodes, Applied Surface Science, 251 (2005) 130-133.
[11] J. Stapelfeldt, J. Wörmer, T. Möller, Evolution of Electronic Energy Levels in Krypton Clusters from the Atom to the Solid, Physical Review Letters, 62 (1989) 98-101.
[12] M. Giuliano, Auger parameter and Wagner plot in the characterization of chemical states by X-ray photoelectron spectroscopy: a review, Spectrosc. Relat. Phenom, 95 (1998) 95-144.
[13] S.J. Morgan, R.H. Williams, J.M. Mooney, An XPS study of thin Pt and Ir silicide overlayer formation on Si(100)2 X 1 surfaces, Applied Surface Science, 56-58 (1992) 493-500.
[14] R. Reiche, S. Oswald, K. Wetzig, XPS and factor analysis for investigation of sputter-cleaned surfaces of metal (Re, Ir, Cr)–silicon thin films, Applied Surface Science, 179 (2001) 316-323.

[15] M.J. Gladys, I. Ermanoski, G. Jackson, J.S. Quinton, J.E. Rowe, T.E. Madey, A high resolution photoemission study of surface core-level shifts in clean and oxygen-covered Ir(2 1 0) surfaces, Journal of Electron Spectroscopy and Related Phenomena, 135 (2004) 105-112.
[16] M. Bianchi, D. Cassese, A. Cavallin, R. Comin, F. Orlando, L. Postregna, E. Golfetto, S. Lizzit, A. Baraldi, Surface core level shifts of clean and oxygen covered Ir(111), New Journal of Physics, 11 (2009) 063002-063002.
[17] J. van der Veen, F. Himpsel, D. Eastman, Structure-Dependent 4f—Core-Level Binding Energies for Surface Atoms on Ir(111), Ir(100)-(5 × 1), and Metastable Ir(100)-(1 × 1), Physical Review Letters, 44 (1980) 189-192.
[18] H. Vuori, A. Pasanen, M. Lindblad, M. Valden, M.V. Niemelä, A.O.I. Krause, The effect of iridium precursor on oxide-supported iridium catalysts prepared by atomic layer deposition, Applied Surface Science, 257 (2011) 4204-4210.
[19] C.Q. Sun, Size dependence of nanostructures: Impact of bond order deficiency, Progress in Solid State Chemistry, 35 (2007) 1-159.
[20] M.A. Omar, Elementary Solid State Physics: Principles and Applications, Addison-Wesley, New York, 1993.
[21] M. Gu, C. Sun, Z. Chen, T. Au Yeung, S. Li, C. Tan, V. Nosik, Size, temperature, and bond nature dependence of elasticity and its derivatives on extensibility, Debye temperature, and heat capacity of nanostructures, Physical Review B, 75 (2007) 125403-125403.
[22] Y. Wang, Y.G. Nie, J.S. Pan, L.K. Pan, Z. Sun, L.L. Wang, C.Q. Sun, Orientation-resolved 3d5/2 binding energy shift of Rh and Pd surfaces: anisotropy of the skin-depth lattice strain and quantum trapping, Physical Chemistry Chemical Physics, 12 (2010) 2177-2182.
[23] N.T. Barrett, C. Guillot, B. Villette, G. Tréglia, B. Legrand, Inversion of the core level shift between surface and subsurface atoms of the iridium (100)(1 × 1) and (100)(5 × 1) surfaces, Surface Science, 251 (1991) 717-721.
[24] M.J. Gladys, I. Ermanoski, G. Jackson, J.S. Quinton, J.E. Rowe, T.E. Madey, A high resolution photoemission study of surface core-level shifts in clean and oxygen-covered Ir(2 1 0) surfaces, Journal of Electron Spectroscopy and Related Phenomena, 135 (2004) 105-112.
[25] W. Hetterich, C. Höfner, W. Heiland, An ion scattering study of the surface structure and thermal vibrations on Ir(110), Surface Science, 251 (1991) 731-736.
[26] C.M. Chan, E.D. Williams, W.H. Weinerg, DEBYE TEMPERATURES OF THE (110) AND (111) SURFACES OF IRIDIUM BY LEED Surface Science, 82 (1979) 577-581.
[27] G.T. Furukawa, M.L. Reilly, J.S. Gallagher, Critical Analysis of Heat: Capacity Data and Evaluation of Thermodynamic Properties of Ruthenium, Rhodium, Palladium, Iridium, and Platinum from 0 to 300K., J. Phys. Chem, Ref. Data 3 (1974) 164-209.